Science and Applications of Energy Beam Ablation

Ronald M. Gilgenbach, *Senior Member, IEEE,* Scott D. Kovaleski, J. S. Lash, Lay-Kee Ang, and Y. Y. Lau

(Invited Review)

***Abstract*—This article reviews the advances in the science and applications of energy beam ablation of materials at the University of Michigan. Types of energy beams applied to materials ablation are: excimer lasers, laser-ablation-assisted plasma discharges, and channelspark electron beams. The characteristics of the ablation plasma plumes generated by these energy deposition sources are discussed and compared. Plume expansion velocities are in the range of cm/μs for all three types of ablation plumes. Electron beam ablation plumes show higher ionization states than laser ablation plumes.**

***Index Terms*—Ablation, e-beam, laser-ablation.**

I. Introduction

THERE has been a rapid increase in the utilization of directed energy technologies in the manufacturing industry. In particular, applications of high power lasers for automobile manufacturing have seen a significant increase for processes including heat-treating, welding, and cutting. Many of these higher power (>1 MW/cm^2) interactions produce significant plasma density, comprising either the shielding gas ambient or vaporized material [1]. With the increasing use of aluminum in automotive bodies, there is expected to be an even greater increase in the use of laser welding as the most viable automated welding mechanism. Although CO_2 lasers have traditionally been used in these applications, more recently, the kW fiberoptic delivery capabilities of one micron radiation have made the CW YAG laser more versatile, particularly in robotic installations.

Excimer lasers have also been employed in the electronics industry for drilling of polymeric, multilayer, printed circuits boards [1]. In these applications the laser fluence is usually kept sufficiently low that little plasma is generated, although in some cases (PET or polyethylene Terephthalate) a flame is generated by combustion of ablated polymer products [2].

Advanced applications of energy beam ablation include deposition of thin films (Fig. 1) [3]. Energy beams are attractive for this application because they can ablate virtually any solid material. Stoichiometry of compounds (e.g., $YBa_2Cu_3O_{7-x}$) is preserved. Alloys can be produced, and high energy ions are generated which are believed to be beneficial to the growth of unique materials (e.g., cubic BN). Potential applications include hardened coatings for gears, substrates for electronics (with high thermal conductivity, e.g., AlN), and diffusion barriers for electronics, (e.g., TiN). Most ablative deposition experiments have utilized pulsed excimer lasers [3].

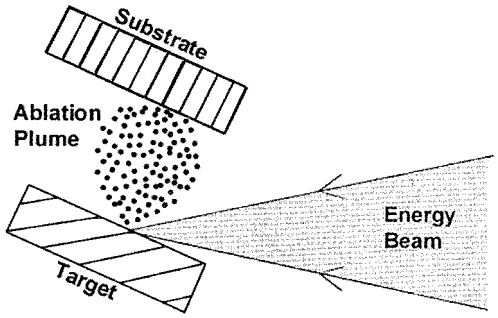

Fig. 1. Experimental configuration for energy beam ablative deposition.

Recently, electron beam ablative deposition has demonstrated potential advantages over laser ablation, including [4]–[7]:

1) high electrical efficiency ($\sim$30%);
2) efficient energy absorption for all materials, (even those that are transparent, e.g., fused SiO_2), or reflecting to laser light;
3) environmentally benign compared to excimer lasers (no toxic gases, such as F or Cl); and
4) low capital cost of e-beam generators compared to lasers.

The first electron beam ablation experiments were performed in Germany [4], [6]. Electron beam ablation research in the U.S. is underway at the University of Michigan [5] and at the Naval Research Laboratory [7].

II. Energy Beam Ablation Experiments

The experimental research program at the University of Michigan has investigated three types of energy beam ablation:

1) excimer lasers (KrF and XeCl), [1], [2], [5], [8]–[12];
2) laser-ablation-assisted-plasma discharges (LAAPD) [13]–[16];
3) electron beams (from a channelspark) [5].

Parameters of the three types of energy beams at the University of Michigan are summarized for comparison in Table I.

The KrF laser operates at wavelength of 248 nm, peak power of <50 MW, energy-per-pulse of <1 J, pulselength of 40 ns, and incident fluence of $\sim$6 J/cm^2. A XeCl laser (308 nm) operates with lower pulse energy (100 mJ), but with a smaller focal spot, yielding a similar fluence of 6 J/cm^2. The

Manuscript received July 22, 1998; revised October 19, 1998. This work was supported by the National Science Foundation. The work of S. D. Kovaleski was supported in part by a DoD/Army AASERT Grant. The work of J. S. Lash and Lay-Kee Ang was supported in part by Sandia National Laboratory.

R. M. Gilgenbach, S. D. Kovaleski, L.-K. Ang, and Y. Y. Lau are with the Intense Energy Beam Interaction Laboratory, Nuclear Engineering and Radiological Sciences Department, University of Michigan, Ann Arbor, MI 48109-2104 USA (e-mail: rongilg@eumich.edu).

J. S. Lash is with Sandia Labs, Albuquerque, NM 87123 USA.

Publisher Item Identifier S 0093-3813(99)02288-2.

TABLE I
TYPICAL PARAMETERS OF ENERGY BEAM ABLATION

	Excimer Laser	LAAP Discharge	Electron Beam
peak power (MW)	25	1.3	<15
energy/pulse (J)	0.1-1	3	1
pulselength (ns)	40	6,000	200
power density (W/cm^2)	10^9	10^8	$<10^9$
energy fluence (J/cm^2)	6-10	---	<30
penetration depth (μm)	0.01-0.1	---	0.5-2
energy density (MJ/cm^3)	3-30	---	<0.5

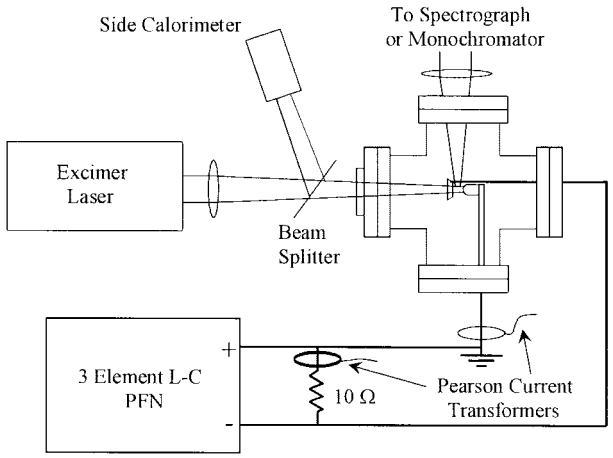

Fig. 2. LAAPD simplified experimental configuration.

penetration depth of ultraviolet laser radiation is limited to the skindepth, typically from 0.01–0.1 μm for metals [5].

LAAPD were investigated as a means of increasing the ionization fraction [13]–[15] of ablation plumes, utilizing inexpensive discharge energy to supplement expensive laser energy, and to promote gas-plasma-phase reactions (e.g., Al + O) [16]. Although the initial intent was to vaporize particulate, this effect was not seen. The experimental configuration for LAAPD is depicted in Fig. 2. The parameters of the LAAPD experiment are: peak voltage of 1.4–3.6 kV, current of 800 A, with a peak power of about 1 MW, and a pulselength of 6 μs (half cycle).

The channelspark electron beam generator was obtained from Forschungszentrum Karlsruhe, Germany [4]. Fig. 3 shows a schematic drawing of the electron beam ablation experiment. The channelspark operates at a charging voltage of negative 15–20 kV, typically generating about 1.5 kA for a 200 ns fullwidth (10–10%) pulse. The energy output is approximately 1 J, or roughly 30% electrical efficiency. Detailed electrical schematics and diagnostics of this device are presented in [4].

Transport and focusing of the electron beam was accomplished by ion-focused-regime (IFR) propagation in the low pressure (5–30 mtorr) gas background, as depicted schematically in Fig. 4. The standard condition for ion-focused transport, in which the electrostatic repulsion force is balanced by the magnetic pinch force [17], is given by the expression

$$f = n_i/n_e = 1/\gamma^2 \tag{1}$$

where γ is the relativistic factor

$$\gamma = 1 + V_e/511\ \text{kV}. \tag{2}$$

For the peak e-beam energy (V_e) of 15 kV, γ is equal to 1.029, requiring a space charge neutralization factor

$$f = n_i/n_e = 0.94. \tag{3}$$

For the current density of the electron beam, typically 50 kA/cm^2, the ion-focused transport requires a gas pressure of about 10 mtorr, close to the operating conditions of the channelspark. This estimate assumes only single ionization; our spectroscopic experiments have detected ion charge states up to +3 in the argon fill gas.

Penetration of the ($\sim$15 kV) electron beam is defined by the stopping power (dE/dx) in the material, typically peaking at $\sim$0.2 μm for iron. Modeling with Sandia National Lab's ITS code [18] shows that some fraction, (typically about 28% at 45 degree incidence), of the electron beam is also reflected (backscattered) out of the material, with the remaining 72% of the energy absorbed within about 0.6 μm of the surface (for iron).

In order to study the science and applications of energy beam ablation, a large array of diagnostics has been developed, as summarized in Table II. These diagnostics have permitted measurements of electron density [1], electron temperature [15], neutral atom density [11], [12], ion density [15], plasma expansion velocities [2], [8], plume dynamics [1], [2], [8]–[12], [15], [19], and particulate relative density and time of flight velocity [20].

Measurements of fundamental species by these diagnostics have permitted study of the dynamics of energy beam ablation, including:

1) thermodynamics [2], [19] (see Section V);
2) hydrodynamics, [2], [8]–[12];
3) ionization dynamics [14], [15];
4) particulate formation and expansion [20].

An additional diagnostic includes optical and electron microscope analysis of targets and ablation deposited films. These are particularly useful for determining the origin and size distribution of particulate [20].

III. EXPERIMENTAL RESUTLS OF LASER ABLATION VERSUS LASER ABLATION ASSISTED DISCHARGES

A series of detailed diagnostic experiments were performed by Lash and Gilgenbach to characterize and compare the plasma plume parameters of laser ablation plumes to those generated by LAAPD [1], [13]–[15]. These diagnostics included both integrated and time-resolved visible spectroscopy,

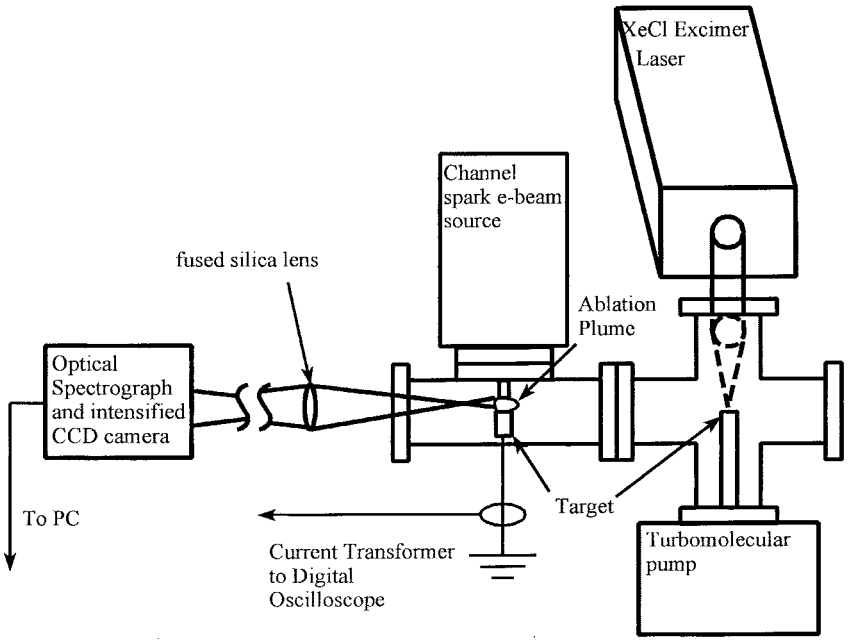

Fig. 3. Experimental configuration for material ablation by channelspark or laser.

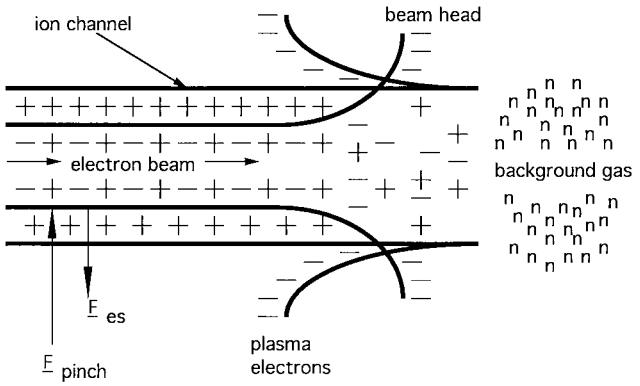

Fig. 4. Schematic illustration of ion focused electron beam transport in a low pressure gas.

TABLE II
DIAGNOSTICS OF ENERGY BEAM ABLATION

diagnostic	parameters measured	references
1) laser deflection	electron/neutral density gradients	1,9,11,12,17
2) schlieren photography	2-D density gradients	2,10
3) optical emission spectroscopy, gated CCD	species identification	13,14,16
4) dye-laser-resonance absorption-photography (DLRAP)	species-resolved dynamics	8,10,12
5) resonant dye-laser interferometry	ion, neutral atom densities, dynamics, electronic temperature	11,12,15
6) dye laser scattering	particulate density, TOF velocity	20
7) double Langmuir probe	electron & ion densities, temp.	15

laser deflection, dye laser resonance absorption photography (DLRAP) [8], and a new resonant ultraviolet interferometry (RUVI) diagnostic [15] developed during this study. The goal of this work was to demonstrate the utility of the LAAPD for energy beam ablation applications as well as ion source applications. Specifically, this effort was concentrated on investigating the ionization dynamics during the ablation of aluminum and iron.

The first diagnostic employed for investigation of the laser ablation plume/plasma and the discharge plasma was time-integrated optical emission spectroscopy (OES) [13], [14]. This diagnostic was chosen for its ease of implementation, noninvasive application, and utility in providing immediate confirmation of the existence of both neutral and ionized species. Aluminum laser ablation plume spectra indicate significant singly-ionized aluminum atom emission at early times ($<$100 ns), while spectra taken with a delay of 140 ns show only ground-state aluminum neutral optical emission transitions. This indicates that for laser ablation of aluminum at a fluence of 4 J/cm^2, the plume contains a significant number of emitting ions which, beyond a few hundred nanoseconds, either cool off so they are not emitting, or recombine with electrons and become a minor plume constituent compared to neutral aluminum atoms.

With application of the 7500 V laser-ablation-assisted discharge, the aluminum plume optical emission is dominated by transitions from singly-ionized (Al_{II}) and doubly-ionized (Al_{III}) species. Additionally, the ground-state neutral optical emission intensity is approximately unchanged from the laser ablation case, leading to the conclusion that most of the plume's neutral atoms were ionized by the discharge. Using the relative line emission intensities, an electronic temperature can be determined for the emitting species. This temperature corresponds to the distribution function describing the bound electron energy level populations. For the 7500 V LAAPD, transitions from Al_{II} ions yield an average electronic temperature of $\sim$1 eV, while transitions from Al_{III} ions provide an average electronic temperature of $\sim$3 eV. Since local thermodynamic equilibrium (LTE) is applicable for the

transitions observed, an average LAAPD electron temperature of 1–3 eV is inferred. This variation in plume temperature may possibly be explained by the time-integrated spectra disguising that the Al_{II} ions are created early during the discharge when the temperature is $\sim$1 eV while the creation of the Al_{III} ions, at a later time, may require a higher temperature near 3 eV.

Time-integrated OES was also performed with an iron target yielding similar results [14]. For laser ablation only, the plume optical emission spectrum is dominated by iron neutral atom transitions with some singly-ionized optical emission. Application of the discharge results in no change in the neutral atom optical emission and a substantial increase in singly-ionized iron atom optical emission. As in the case of aluminum, this implies that more ions are being created with the discharge. Due to difficulty resolving the individual iron singly-ionized transitions, an electronic temperature was only determined for the iron neutral atoms generated in the laser ablation plume. The inferred temperature was 0.5 eV, which, since LTE was applicable, implies an average iron laser ablation plume electron temperature of 0.5 eV.

Qualitative, two-dimensional (2-D) species-specific information was obtained through use of the DLRAP diagnostic. In this diagnostic, the dye laser is tuned to a species resonant transition, thus promoting stimulated absorption of the beam resulting in a "shadow" of the resonant species. Compared with laser ablation, aluminum neutral atom absorption was decreased with application of the discharge indicating a reduction in the relevant neutral atom, excited-state population.

For iron, the same depletion effect was observed with ground-state iron neutral atoms. In contrast to aluminum, a singly-ionized iron atom transition could be probed with the dye laser. Application of the discharge resulted in enhanced iron ion absorption over that observed with only laser ablation. This further strengthens the hypothesis that the discharge increases the ionization in the laser ablation plume. It is also important to note that iron plume expansion is very forward-directed, while the aluminum plume expands strongly in the radial direction; effects that are not understood at this time. Additionally, iron neutral atom absorption was detected as late as 5 μs from laser ablation implying a density of $\sim 10^{12}$ cm^{-3} at this time.

For quantitative verification of the increase in ionization due to the application of the LAAPD, a RUVI diagnostic was developed [15]. This diagnostic provided species-specific, 2-D, absolute line-density profiles of the laser ablation plume and the discharge plasma. In particular, the absolute line-density profiles of two iron neutral and single-ion populations have been measured. The advantage of using two populations in each iron species, is that this allows the neutral and ion electronic temperature, total number of each species, and the ionization ratio to be calculated assuming the energy level populations follow a Boltzmann distribution.

The use of the RUVI diagnostic has provided the first known absolute density measurements of both neutral atoms and ions from a laser ablation plasma [15]. These data are summarized in Table III. Iron neutral ground-state atomic line densities up to 5.9×10^{14} cm^{-2} have been measured and singly-ionized, excited-state ion line densities above 1×10^{15} cm^{-2} have been observed. These measurements imply a plume density of $\sim 1 \times 10^{15}$ cm^{-3} even as late as 400 ns with a fluence of $\sim$7 J/cm^2. Through line-density measurements of two species populations and assumption of a Boltzmann population distribution, species electronic temperatures have been inferred. Iron neutral atom electronic temperatures of 1.0 eV (400 ns) to 0.6 eV (800 ns) have been measured from laser ablation while with application of the discharge, these temperatures increase by approximately 0.2 eV. Singly-ionized iron atom temperatures of 0.5 eV (600 ns) to 0.25 eV (1200 ns) have been observed from laser ablation while the ion temperature increases to 0.8 eV during the discharge. These temperatures ($\sim$1 eV) and ion densities (5×10^{14} cm^{-2}) are in good agreement with values obtained from floating, double-Langmuir probe measurements [14]. (Higher plasma densities (10^{16}–10^{18} cm^{-3}) are typically measured closer to the surface, before plume expansion has occurred) [1]. By following the expansion of single equiline-density contours, an iron neutral plume expansion velocity of 1.8 cm/μs and iron ion plume expansion velocity of 3.5 cm/μs have been determined. With the high laser fluences used in this work, the laser ablation plume ionization ratio (the total number of Fe_{II} ions divided by the total number of Fe_I neutral atoms) at 1200 ns after the excimer laser pulse is approximately four. The high laser ablation ionization fraction may be the result of a resonant interaction effect of the KrF excimer laser and iron neutral atom transitions near 248 nm. With application of the discharge, the ionization ratio increases by a factor of $\sim$5 to an ionization ratio of approximately 20, quantitatively proving that the LAAPD enhances the laser ablation plume ionization.

TABLE III
SUMMARY OF IONIZATION DYNAMICS EXPERIMENTS ON LASER ABLATION PLUMES VERSUS LASER ABLATION ASSSISTED PLASMA DISCHARGES

Parameter	Laser Ablation	LAAPD
number of Fe atoms (N_n)	1.4×10^{14}	0.4×10^{14}
number of Fe ions (N_i)	5×10^{14}	7×10^{14}
ionization ratio (N_i/N_n)	3.6	18
electronic temperature (from FeII)	0.25 eV	0.8 eV

IV. ELECTRON BEAM ABLATION EXPERIMENTAL RESULTS

Electron beam ablation experiments at UM have been conducted on pure metals (Fe and Ti), a conducting compound (TiN), and an insulating compound (fused-silica, SiO_2). Spectroscopic emission measurements of Fe ablation by electron beams were compared to XeCl excimer laser ablation in a previous article [5]. Those previous data showed that e-beam ablation yielded much higher ionization of Fe plumes than laser ablation. In this article we present the results of temporally-resolved optical/spectroscopic measurements of electron beam ablated Ti, TiN, and SiO_2.

DLRAP of e-beam-ablated Si neutral atom plumes from a fused silica target are presented in Fig. 5. These DLRAP data were measured by tuning the dye-laser to the 288.158

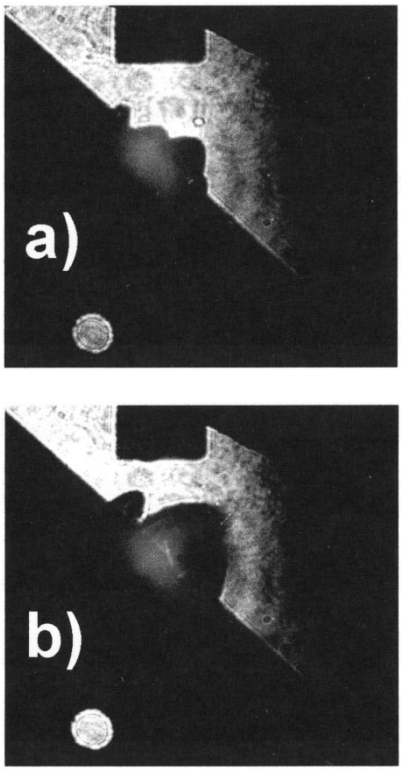

Fig. 5. DLRAP (288.158 nm resonance line) of silicon neutral atom plume expansion, taken at (a) 400 ns and (b) 600 ns.

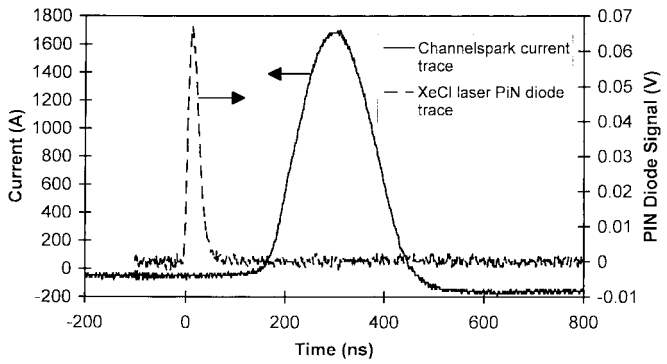

Fig. 6. Pulse shapes of channelspark electron beam compared to XeCl excimer laser.

nm neutral absorption line of silicon. From the photographs at different times (only two shown), one can estimate the expansion velocity of the electron beam-ablated Si neutral atom plume at about 1 cm/μs, comparable to previous laser ablated metal atom plumes at fluences of a few J/cm^2 [8], [11].

Fig. 6 depicts the temporal pulse shapes for the electron beam (target current) versus the XeCl laser for comparison. The fullwidth (FW) of the e-beam current is about 200 ns, compared to about 40 ns (FW) for the laser. These and previous spectroscopic measurements showed bright optical emission from the argon plasma (up to $+3$ ionization states), which strongly competes with the ablation plume light in spectroscopic measurements. This Ar background plasma emission peaks strongly during the e-beam pulse.

Fig. 7 presents temporally-resolved spectra of three emission lines (neutral, singly-ionized, and doubly-ionized) titanium ablation by the e beam. In contrast to the interfering

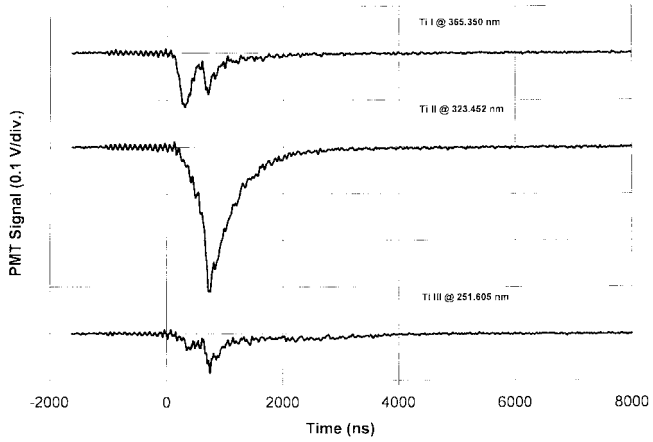

Fig. 7. Temporally resolved spectroscopic emission from e-beam ablation of titanium metal target. Ti neutral, singly-ionized, and doubly ionized lines shown. The initial spike on Ti_I line is probably interfering argon line during e-beam pulse.

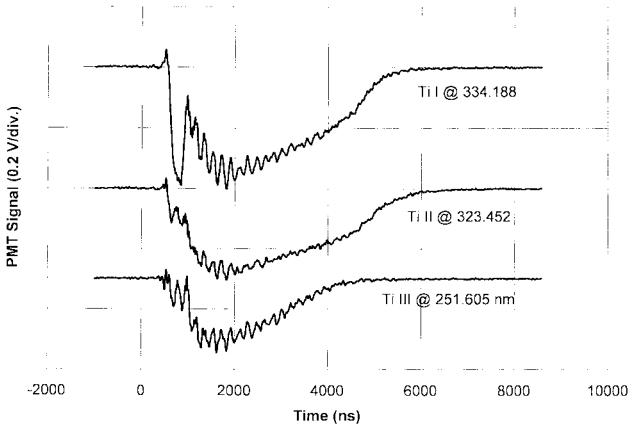

Fig. 8. Temporally resolved spectroscopic emission from e-beam ablation of titanium-nitride target. Ti neutral, singly-ionized, and doubly ionized lines shown. The initial spike on Ti_I line is probably interfering argon line during e-beam pulse.

argon line (the initial pulse that resembles the e-beam current in the top trace), the Ti_I plume emission peaks after the e-beam current pulse has ended. This effect is believed due to the plume atom/ion expansion velocity (estimated at about 1 cm/μs) into the monochromator field of view ($\sim$1 cm diameter circle tangent to the target). The most intense optical emission is from the singly-ionized (Ti_{II}) line at 323.452 nm, where the neutral and doubly-ionized peaks were much weaker. All three Ti lines peak at about 860 ns after the peak e-beam current. The Ti optical emission persists for some 2 μs after the e-beam current peak.

Titanium-nitride ablation exhibited different spectroscopic emission than pure Ti metal. Fig. 8 gives the temporal evolution of titanium neutral, singly-ionized, and doubly-ionized emissions in the e-beam ablated plume. The temporal response of the TiN ablation plume optical emission is much slower and peaks at a later time (950 ns after e-beam peak current) than the Ti metal case. The optical emission from neutral and singly (doubly) ionized Ti lines persists for a much longer time, 5 μs (4 μs) than for Ti metal. The reason for this much different behavior is unknown at this time, but it is conjectured that this effect is related to the ablation mechanism and lower thermal

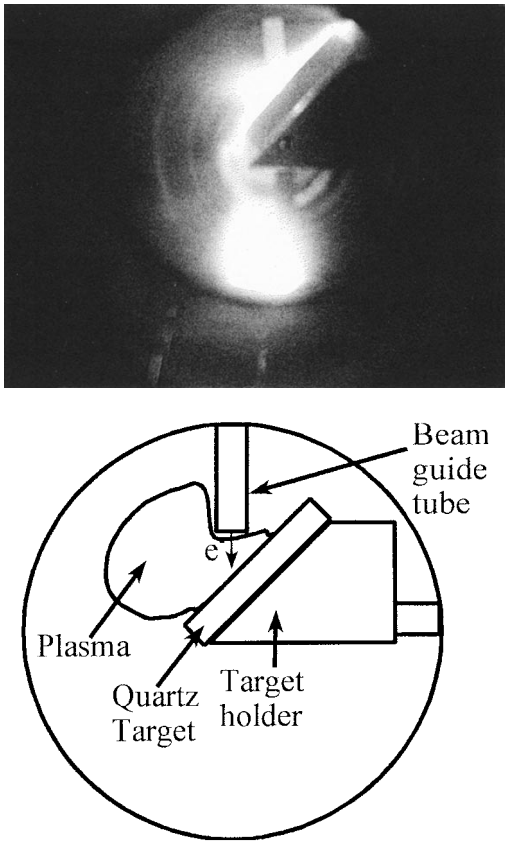

Fig. 9. Open shutter photograph of e-beam ablation of fused silica target.

conductivity of the sintered TiN target. This remains an area of further study.

The ablation of an insulating compound, SiO_2 presented an intriguing example of electron beam ablation, since there is no direct return current path for the electrons to flow to ground. This unique behavior is presented in the open shutter photograph of Fig. 9. It can be seen that the plasma builds up on the surface of the SiO_2 target, to a much larger extent than conducting targets. Furthermore, the bright flash from the target to the chamber apparently indicates that the SiO_2 surface charges from the e-beam current until it reaches a sufficient voltage to arc to the grounded chamber. This arcing thus provides the necessary return current path for the electron beam.

Spectroscopic Si emission lines from SiO_2 ablation by an electron beam are presented in Fig. 10. The emission from Si neutral atoms and singly/doubly-ionized ions differs from the previous case in several respects. First, the peak Si emission occurs near the time of the peak electron beam current. Second, the intensity of all three Si emission lines is significantly higher than the conducting materials. The neutral and singly-ionized lines persist longer ($\sim$4 μs) than the doubly ionized lines.

The higher plume optical emission intensity from SiO_2 ablation could be due to the fact that the thermal conductivity of SiO_2 (0.0148 W cm^{-1} K^{-1} at 100C) is much less than Fe (0.720 W cm^{-1} K^{-1}) or Ti (0.207 W cm^{-1} K^{-1}). It should be noted that the ablation rate of SiO_2 is sufficiently high that thin films have recently been deposited onto copper substrates with about 5000 pulses.

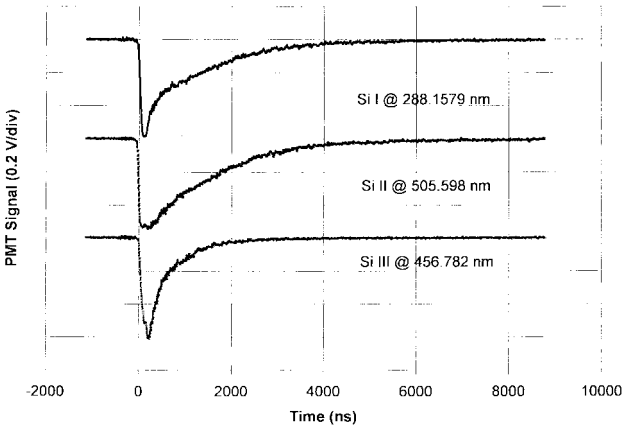

Fig. 10. Temporally resolved spectroscopic emission from e-beam ablation of SiO_2 target. Si neutral, singly-ionized, and doubly ionized lines shown.

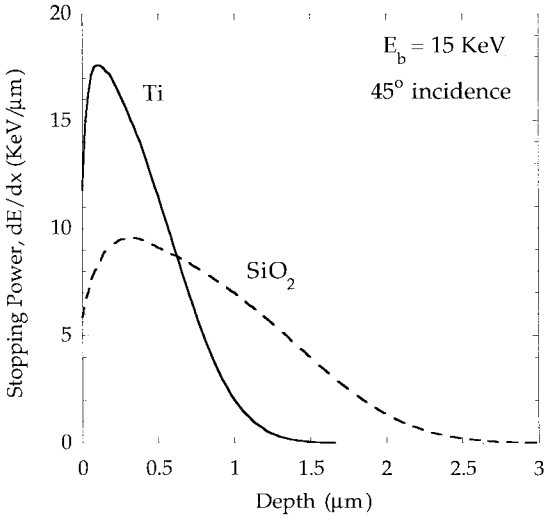

Fig. 11. Stopping power of a 15 keV pencil electron beam impinging on Ti and fused silica, with 45° incidence. (From ITS Tiger code [18].)

V. Thermodynamics of Electron Beam Ablation Versus Laser Ablation

The thermodynamics of electron beam ablation differs significantly from laser ablation. The fundamental difference is that the electron penetration depth (range) in the target is much greater than the skin depth in laser ablation (Table I). In the specific case of channelspark e beam versus excimer laser, the e-beam pulselength is in addition five times longer, so there is more time for thermal diffusion to greater depths. Both of these effects increase the effective depth of energy deposition for the e beam, delaying the onset time for vaporization and plasma formation.

We use the one-dimensional heat diffusion equation [21]–[22] to calculate the spatial and temporal evolution of the target's temperature $T(x,t)$ under the irradiation by the XeCl (308 nm, 40 ns) laser and the channelspark electron beam (15 keV, 200 ns). We use the output of the ITS-Tiger Monte-Carlo code [18] (described below) for the source term. The targets are pure Ti and fused silica (SiO_2), and the laser or electron beam is incident with an angle of 45° from the normal axis. In the calculation, we assume that the target undergoes normal vaporization [23], [24] at the outer surface,

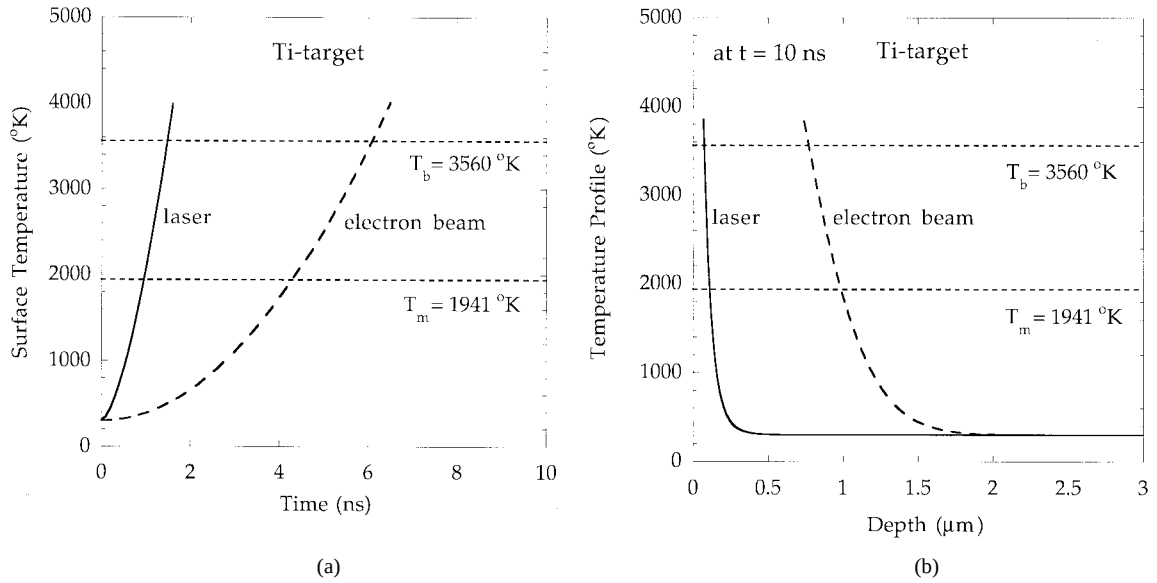

(a) (b)

Fig. 12. (a) Surface temperature as a function of time of a Ti-target irradiated by XeCl laser (308 nm) and channelspark electron beam (15 keV), with a peak power density of 2500 MW/cm^2, where T_b = boiling temperature and T_m = melting temperature. (b) Temperature profile at t = 10 ns of a Ti-target irradiated by XeCl laser (308 nm) an channelspark electron beam (15 keV), with a peak power density of 2500 MW/cm^2, where T_b = boiling temperature and T_m = melting temperature.

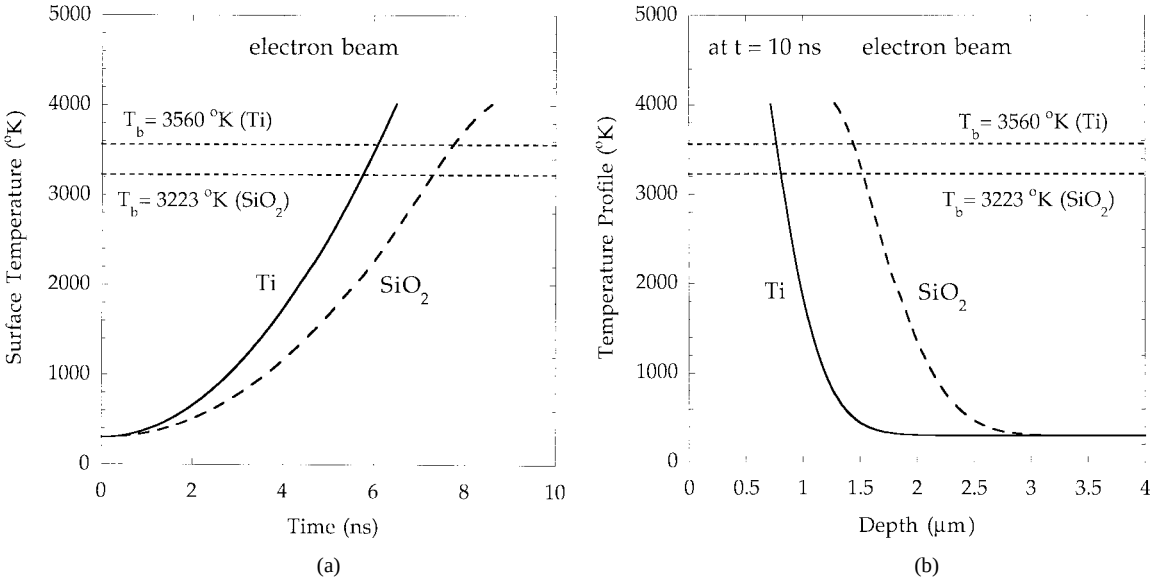

(a) (b)

Fig. 13. (a) Surface temperature as a function of time of a Ti-target and fused silica irradiated by channelspark electron beam (15 keV), with a peak power density of 2500 MW/cm^2, where T_b = boiling temperature. (b) Temperature profile at t = 10 ns of a Ti-target and fused silica irradiated by channelspark electron beam (15 keV), with a peak power density of 2500 MW/cm^2, where T_b = boiling temperature.

and consider the energy balance at the phase transitions. From our experimental results, we approximate the laser (electron beam current) pulse's temporal shape as triangular (sine) function (see Fig. 6), with a peak power density $P_o = 2500$ MW/cm^2 at mid pulse, $t = 20$ ns (100 ns). The laser energy is deposited into the target's surface following the Beer's law $(A\mu P_o \exp(-\mu x))$, where A is the optical absorptivity on the surface and μ is the inverse of the skin depth δ. Under 308 nm laser irradiation on a Ti-target, $A = 0.43$ and $\delta = 15$ nm.

In Fig. 11, the stopping power dE/dx of a 15 keV pencil electron beam with 45° incidence for both Ti and SiO_2 is calculated from the ITS-Tiger Monte-Carlo code [18]. Here, the SiO_2 is assumed to be a pure insulator. The fraction of total energy absorption of the electron beam in the target is determined by integrating dE/dx in Fig. 11. The energy absorption fraction is 0.75 (0.86) for Ti (SiO_2). Because Ti has a higher atomic number and atomic mass, the electrons penetrate less deeply in Ti than SiO_2. Finally, the source term in the heat diffusion equation for the electron beam is then expressed as $1/E_b(dE/dx)P_o$, where $E_b = 15$ keV. For simplicity we assume that the thermophysical properties of the targets are temperature independent.

As the effects of beam-plasma interaction and the gas dynamics are not included, the target's temperature evolution and profile are shown only up to about the boiling temperature T_b. In Fig. 12, we show the temporal evolution of the temperature on the target's surface [Fig. 12(a)] and spatial temperature distribution [Fig. 12(b)] at time 10 ns, of Ti for both laser

and electron beam irradiation. In Fig. 12(a), after t greater than 1.5 ns (6 ns), the surface temperature of Ti surpasses T_b for laser (electron beam) irradiation. At 10 ns, Fig. 12(b) indicates that the electron beam is expected to have a larger evaporation depth than the laser, i.e., about 0.1 μm (laser) and 0.8 μm (electron beam). One of the main advantages of electron beam ablation is the capability of ablating transparent materials (e.g., fused silica). In Fig. 13, we show the temporal and spatial evolution of temperature for SiO_2. Due to its lower atomic number and deeper stopping power of SiO_2, shown in Fig. 11, SiO_2 has a slower surface temperature rise [Fig. 13(a)] and larger evaporation depth [Fig. 13(b)] than Ti. Thus, fused silica can be ablated after only 7 ns irradiation by a 15 keV, 200 ns channelspark electron beam source.

Laser effects which have not been modeled here are the increased absorption due to surface roughness [25] nor multipulse surface instabilities [26].

Electron beam effects which have not been modeled here are channelspark e-beam voltage collapse and surface charging of the SiO_2. Such charging may cause electron beam instabilities, a possible cause of the multiple plumes seen in Fig. 5 [27].

Particulate production by energy beam ablation is one of the most critical aspects in thin film deposition. A comparison was made by Lash between laser and LAAPD, but a quantitative, real-time measurement of e-beam ablated particulate has not yet been completed. Lash's real-time laser scattering from particulate showed little difference (within the error bars) for laser ablation compared to LAAPD. Initial electron microscopy of e-beam ablated targets and deposited films showed the presence of submicron droplets. It is believed that these droplets originate from observed surface melting within the micron electron range in materials. Since the laser ablation skin depth is typically more shallow for metals, the e-beam has more potential to generate droplets for undamaged targets.

VI. Future Directions of Energy Beam Ablation Research

The future of energy beam ablation research is fertile in new approaches, including:

1) free electron laser (FEL) ablation [28];
2) copper vapor laser ablation; and
3) new electron beam sources.

A particularly significant, new experiment on FEL ablation is planned for the FEL group at the Jefferson Lab [28]. The FEL's wavelength tuneability and ultra-short pulse will make this a major testbed for topics, such as wavelength scaling, resonant interactions with materials, and effects of ultrashort pulselengths. Ultra-short pulses could reduce the particulate, typically generated by longer-pulse laser ablation, because the penetration depth due to thermal conductivity is negligible during the pulse.

Copper vapor lasers developed at Lawrence Livermore National Labs for atomic vapor laser isotope separation [29] have the advantage of small focal spot (green and yellow light) and high repetition rate (1–20 kHz). It is believed that pulsed ablation has the advantage that the plasma plume expels ablated matter from the bore of small holes, yielding very clean, straight sides.

A number of new electron beam sources are being investigated in the former Soviet Union and elsewhere. These will open up new applications for larger area e beams to materials ablation and surface treatment. Commercialization of electron beam ablative thin-film deposition may occur within the next several years [30]. Other laser-sustained-arc discharge research has been performed elsewhere [31].

VII. Summary and Conclusions

The science and applications of energy beam ablation have made great strides during the past decade. Many of the new developments in materials synthesis have relied upon laser ablative deposition. Electron beam ablative deposition is promising, especially for thin films of transparent materials such as SiO_2, as well as Si (recently ablated at UM), which are important to the microelectronics and optoelectronics industries.

Acknowledgment

The authors would like to acknowledge the efforts of former graduate students who contributed to the original development of ablation plume diagnostics, including: P. L. G. Ventzek, R. A. Lindley, M. E. Cuneo, C. L. Enloe, L. D. Horton, J. E. Tucker, H. L. Spindler, and C. H. Ching. The authors also appreciate the stimulating discussions with D. Hinshelwood.

References

[1] R. M. Gilgenbach, C. H. Ching, J. S. Lash, and R. A. Lindley, "Laser diagnostic experiments on KrF laser ablation relevant to manufacturing applications," *Phys. Plasmas*, vol. 1, pp. 1619–1625, May 1994.
[2] P. L. G. Ventzek, R. M. Gilgenbach, J. Sell, and D. Heffelfinger, "Schlieren measurements of the hydrodynamics of excimer laser ablation of polymers in atmospheric pressure gas," *J. Appl. Phys.*, vol. 68, pp. 965–968, Aug. 1, 1990.
[3] *Pulsed Laser Deposition of Thin Films*, D. B. Chrisey and G. K. Hubler, Eds. New York: Wiley, 1994.
[4] G. Muller and C. Schultheiss, "Deposition means of pulsed electron beam ablation," in *Proc. Beams'94*, San Diego, CA, vol. II, pp. 833–836.
[5] S. Kovaleski, R. M. Gilgenbach, L. K. Ang, Y. Y. Lau, and J. S. Lash, "Electron beam ablation versus laser ablation: plasma plume diagnostic studies," *Appl. Surf. Sci.*, vol. 127–129, pp. 947–952, May 1998.
[6] T. Witke, A. Lenk, and B. Schultrich, "Investigation of plasma produced by electron beam ablation," *IEEE Trans. Plasma Sci.*, vol. 24, pp. 61–62, Feb. 1996.
[7] D. Hinshelwood and A. Fisher, private communications, 1997.
[8] R. M. Gilgenbach and P. L. G. Ventzek, "Dynamics of excimer laser-ablated aluminum-neutral-atom plume measured by dye-laser-resonance-absorption photography," *Appl. Phys. Lett.*, vol. 58, pp. 1597–1599, April 15, 1991.
[9] P. L. G. Ventzek, R. M. Gilgenbach, J. A. Sell, and D. Heffelfinger, "Laser beam deflection measurements and modeling of pulsed laser ablation rate and near-surface atom densities in vacuum," *J. Appl. Phys.*, vol. 70, pp. 587–593, July 15, 1991.
[10] P. L. G. Ventzek, R. M. Gilgenbach, C. H. Ching, and R. A. Lindley, "Schlieren and dye laser resonance absorption photographic investigations of KrF excimer laser ablation of polyimide, polyethylelene terephthalate, and aluminum," *J. Appl. Phys.*, vol. 72, pp. 1696–1706, Sept. 1, 1992.
[11] R. A. Lindley, R. M. Gilgenbach, and C. H. Ching, "Resonant holographic interferometry measurements of laser ablation plumes," *Appl. Phys. Lett.*, vol. 63, pp. 888–890, Aug. 16, 1993.
[12] R. A. Lindley, R. M. Gilgenbach, C. H. Ching, J. S. Lash, and G. L. Doll, "Resonant holographic interferometry measurements of laser ablation plumes in vacuum, gas, and plasma environments," *J. Appl. Phys.*, vol. 76, pp. 5457–5472, Nov. 1, 1994.
[13] J. S. Lash, R. M. Gilgenbach, and C. H. Ching, "Laser ablation assisted-plasma-discharges of aluminum in a transverse-magnetic field," *Appl. Phys. Lett.*, vol. 65, pp. 531–533, Aug. 1, 1994.
[14] J. S. Lash, R. M. Gilgenbach, and H. L. Spindler, "Characterization of laser ablation assisted plasma discharge metallic ion source," *Plasma*

Sources Sci. Technol., vol. 4, pp. 511–515, Nov. 1995.
[15] ——, "Ionization dynamics of iron plumes generated by laser ablation versus a laser-ablation-assisted-discharge," *J. Appl. Phys.*, vol. 79, pp. 2287–2295, Mar. 1, 1996.
[16] C. H. Ching, R. M. Gilgenbach, and J. S. Lash, "Detection of AlO molecules produced by KrF laser ablated Al atoms in oxygen gas and plasma environments," *J. Appl. Phys.*, vol. 78, pp. 3408–3410, Sept. 1, 1995.
[17] M. Reiser, *Theory and Design of Charged Particle Beams*. New York: Wiley, 1994.
[18] Integrated Tiger Series (ITS) Codes, Sandia National Laboratories Report no. SAND91-1634.
[19] J. A. Sell, D. Heffelfinger, P. L. G. Ventzek, and R. M. Gilgenbach, "Photothermal and photoacoustic beam deflection as a probe of laser ablation of materials," *J. Appl. Phys.*, vol. 69, p. 1330–1336, Feb. 1, 1991.
[20] H. L. Spindler, R. M. Gilgenbach, and J. S. Lash, "Effects of laser-ablation target damage on particulate production investigated by laser scattering with deposited thin-film and target analysis," *Appl. Phys. Lett.*, vol. 68, pp. 3245–3247, June 3, 1996.
[21] H. S. Carslaw, and J. C. Jaeger, *Conduction of Heat in Solids*. Oxford, U.K.: Clarendon, 1959.
[22] S. I. Anisimov and V. A. Khokhlov, *Instabilities in Laser-Matter Interaction*. Boca Raton, FL: Chemical Rubber, 1995, ch. 1.
[23] A. Miotello and R. Kelly, "Critical assessment of thermal models for laser sputtering at high fluences," *Appl. Phys. Lett.*, vol. 67, pp. 3535–3537, Dec. 11, 1995.
[24] A. Peterlongo, A. Miotello, and R. Kelly, "Laser-pulse sputtering of aluminum: Vaporization, boiling, superheating, and gas-dynamic effects," *Phys. Rev. E*, vol. 50, pp. 4716–4727, Dec. 1994.
[25] L. K. Ang, Y. Y. Lau, R. M. Gilgenbach, and H. L. Spindler, "An analysis of laser absorption on a rough metal surface," *Appl. Phys. Lett.*, vol. 70, pp. 696–698, Feb. 10, 1997.
[26] L. K. Ang, Y. Y. Lau, R. M. Gilgenbach, H. L. Spindler, J. S. Lash, and S. D. Kovaleski, "Surface instability of multi-pulse laser ablation on a metallic target," *J. Applied Physics*, vol. 83, pp. 4466–4471, Apr. 15, 1998.
[27] S. D. Kovaleski, R. M. Gilgenbach, L. K. Ang, and Y. Y. Lau, "Dynamics of electron beam ablation of silicon dioxide measured by dye laser resonance absorption photography," *Appl. Phys. Lett.*, vol. 73, no. 18, pp. 2576–2578, Nov. 2, 1998.
[28] F. Dylla, in *Proc. 5th Free Electron Laser Users Workshop*, Williamsburg, VA, Aug. 19–23, 1998.
[29] B. Warner, private communication, 1994.
[30] T. Venkatesan, private communication, 1998
[31] P. Siemroth and H. J. Sheibe, "The method of laser-sustained arc ignition," *IEEE Trans. Plasma Science*, vol. 18, pp. 911–916, Dec. 1990.

Ronald M. Gilgenbach (S'73–M'74–SM'92) received the Ph.D. degree in electrical engineering from Columbia University, New York, in 1978 and the B.S. and M.S. degrees from the University of Wisconsin, Madison, in 1972 and 1973, respectively.

He joined the faculty of the University of Michigan, Ann Arbor, in 1980 and became Director of the Intense Energy Beam Interaction Laboratory, a post he still holds. He is also a Professor in the Nuclear Engineering and Radiological Sciences Department and in the Applied Physics Program at the University of Michigan. He gained several years of industrial experience at Bell Labs. From 1978–1980, he worked as a Contractor at the Naval Research Laboratory, where he was involved in research and development on the first, long-pulse, 35-GHz gyrotron for plasma heating. He performed experiments on the ISX-B tokamak at Oak Ridge National Laboratory, which represented the first gyrotron electron cyclotron heating experiments on a tokamak in the U.S. His research at the University of Michigan has concentrated on the physics and applications of electron beams and microwaves, as well as laser plasmas, laser diagnostics, and industrial materials processing. He has had research interactions with scientists at Phillips Lab, Sandia National Labs, Northrop–Grumman, General Motors Research Labs, Los Alamos National Lab, Fermilab, and NRL.

Dr. Gilgenbach is Secretary and past member of the Executive Committee of the IEEE Plasma Sciences and Applications Technical Committee. He is a Fellow of the American Physical Society and received the 1997 Plasma Sciences and Applications Award from the IEEE PSAC.

Scott D. Kovaleski received the B.S. degree from Purdue University, West Lafayette, IN, in 1995 and the M.S. degree from the University of Michigan, Ann Arbor, in 1997, both in nuclear engineering.

Since 1995 he has been a Research Assistant in the Intense Energy Beam Interaction Laboratory at the University of Michigan, where he is pursuing the Ph.D. degree. His research interests include the study of electron beam ablation and the application of plasma diagnostics to ablation plumes.

J. S. Lash, photograph and biography not available at the time of publication.

Lay-Kee Ang received the B.S. degree from National Tsinghua University, Hsinchu, Taiwan, R.O.C., in 1994 and the M.S. degree from the University of Michigan, Ann Arbor, in 1996. He is currently working toward the Ph.D. degree at the University of Michigan.

His research interests are in laser ablation of materials, multipactor discharge, and high power microwave source. He has several publications on these subjects.

Y. Y. Lau was born in Hong Kong in 1947. He received the S.B., S.M., and Ph.D. degrees in electrical engineering from the Massachusetts Institute of Technology (MIT), Cambridge, MA, in 1968, 1970, and 1973, respectively.

He was an Instructor and, later, an Assistant Professor in Applied Mathematics at MIT from 1973–1979. He was with Science Applications Incorporation from 1980–1983 and with the Naval Research Laboratory from 1983–1992, both as a Research Physicist. Since 1992, he has been with the University of Michigan, Ann Arbor, as a Professor in the Department of Nuclear Engineering and Radiological Sciences and in the Applied Physics Program. He has worked mostly on electron beams (negative mass, hose, and beam breakup instabilities, beam quality, two-beam accelerators), coherent radiation source (gyro-TWT, gyromagnetron, relativistic klystron, crossed-field sheath), plasmas, and discharges (vacuum arc, laser ablation, multipactor). He holds seven patents and over 100 refereed publications.

Dr. Lau won several invention awards and publication awards while at the Naval Reasarch Laboratory, and was the recipient of the 1989 Sigma-Xi Scientific Society Applied Science Award. He received the 1998 University of Michigan College of Engineering Excellence in Research Award. He was elected Fellow of the American Physical Society in 1986 and currently serves as an Associate Editor of the Physics of Plasmas.